




RESEARCH ARTICLE

 OPEN ACCESS 

## Characterising phagocytes and measuring phagocytosis from live *Galleria mellonella* larvae

Jennie S. Campbell<sup>a</sup>, James C. Pearce<sup>a</sup>, Attila Bebes<sup>b</sup>, Arnab Pradhan<sup>c</sup>, Raif Yuecel<sup>b</sup>, Alistair J P Brown<sup>c</sup>, and James G. Wakefield <sup>a</sup>

<sup>a</sup>Living Systems Institute, University of Exeter, Exeter, UK; <sup>b</sup>Exeter Centre for Cytoomics, Henry Wellcome Building for Biocatalysis, Biosciences, University of Exeter, Exeter, UK; <sup>c</sup>Medical Research Council Centre for Medical Mycology, University of Exeter, Exeter, UK

### ABSTRACT

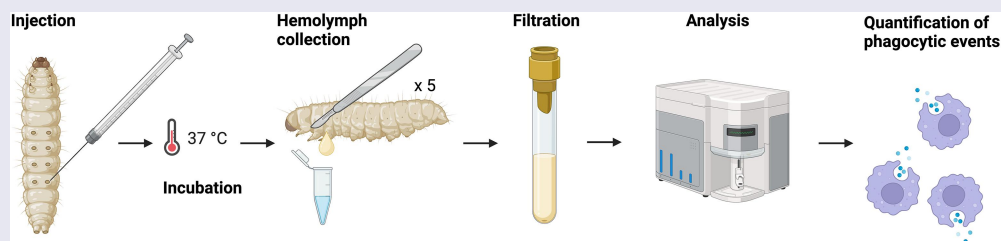
Over the last 20 years, the larva of the greater waxmoth, *Galleria mellonella*, has rapidly increased in popularity as an *in vivo* mammalian replacement model organism for the study of human pathogens. Experimental readouts of response to infection are most often limited to observing the melanization cascade and quantifying larval death and, whilst transcriptomic and proteomic approaches, and methods to determine microbial load are also used, a more comprehensive toolkit of profiling infection over time could transform the applicability of this model. As an invertebrate, *Galleria* harbour an innate immune system comprised of both humoral components and a repertoire of innate immune cells – termed haemocytes. Although information on subtypes of haemocytes exists, there are conflicting reports on their exact number and function. Flow cytometry has previously been used to assay *Galleria* haemocytes, but protocols include both centrifugation and fixation – physical methods which have the potential to affect haemocyte morphology prior to analysis. Here, we present a method for live haemocyte analysis by flow cytometry, revealing that *Galleria* haemocytes constitute only a single resolvable population, based on relative size or internal complexity. Using fluorescent zymosan particles, we extend our method to show that up to 80% of the *Galleria* haemocyte population display phagocytic capability. Finally, we demonstrate that the developed assay reliably replicates *in vitro* data, showing that cell wall  $\beta$ -1,3-glucan masking by *Candida albicans* subverts phagocytic responses. As such, our method provides a new tool with which to rapidly assess phagocytosis and understand live infection dynamics in *Galleria*.

### ARTICLE HISTORY

Received 30 October 2023  
Revised 17 January 2024  
Accepted 29 January 2024

### KEYWORDS

*Galleria mellonella*; 3Rs; replacement model; flow cytometry; phagocytosis; infection; *Candida albicans*




## Introduction

Larvae of the greater waxmoth, *Galleria mellonella*, are rapidly gaining popularity as the mammalian replacement model organism of choice to study a variety of human pathogens to which they are susceptible [1–8]. This is due both to their relatively large size – up to 2.5 cm [9] – which makes them amenable to handling and accurate dosing, and to their viability at 37 °C (i.e. human physiological temperature).

As an invertebrate, *Galleria mellonella* is equipped with an innate immune system – which, like that of

mammals, consists of both humoral and cellular responses. A major humoral immune response is the induction of the melanization cascade. This cascade, which is initiated by the presence of both microbial compounds [10] and physiological stressors, causes *Galleria* larvae to turn black following the activation of phenoloxidase, and the melanin produced then aids in the trapping and killing of pathogens [11]. The phenotypic change from a healthy cream colour to a darker brown/black can be scored for simple health readouts from infection experiments [12], while

**CONTACT** James G. Wakefield  [j.g.wakefield@exeter.ac.uk](mailto:j.g.wakefield@exeter.ac.uk)

 Supplemental data for this article can be accessed online at <https://doi.org/10.1080/21505594.2024.2313413>

© 2024 The Author(s). Published by Informa UK Limited, trading as Taylor & Francis Group.  
This is an Open Access article distributed under the terms of the Creative Commons Attribution License (<http://creativecommons.org/licenses/by/4.0/>), which permits unrestricted use, distribution, and reproduction in any medium, provided the original work is properly cited. The terms on which this article has been published allow the posting of the Accepted Manuscript in a repository by the author(s) or with their consent.

microbial load can be assessed through *ex vivo* plating and CFU counting of the pathogen [e.g. 7] but these provide only rudimentary scores of health status.

More detailed cellular and molecular responses to infection in *Galleria*, analogous to mammalian systems, have been developed. Larvae generate an array of antimicrobial peptides (AMPs), secreted from both the fat body, which is the equivalent to the mammalian liver and adipose tissue, and the cells of the insect immune system to combat infection [13–17]. Techniques including rt-/q-PCR and comparative proteomics/transcriptomics can be used to understand the humoral responses of *Galleria* larvae to infections and physiological stressors [3,5,17–19]. However, due to a distinct lack of experimental tools – such as antibodies which might recognize specific cell populations activated upon infection – more straight-forward techniques to monitor the immune response and levels of AMPs in *Galleria*, such as immunofluorescence and Western Blotting, are not widely applicable.

The cellular components of the *Galleria* immune system are innate immune cells (termed haemocytes) that are found predominantly within the haemolymph that circulates through the haemocoel. However, further populations are also found within certain tissues such as the fat body, haemopoietic organ and as sessile populations attached to the cuticle, as with other lepidoptera species [20]; reviewed in [21]. Haemocytes perform three major immune functions – phagocytosis, encapsulation and induction of the melanisation cascade [15,22,23], and are also involved in production of lipid transport and storage proteins [24,25] – thus, they also play a role in the metabolism of the larva. *Galleria* haemocytes were first observed and characterized in 1977– with five cell subtypes being identified [26]. Of these, plasmatocytes and granulocytes (the most abundant) display phagocytic capability *in vitro* [23]. The phagocytic rate of *Galleria* haemocytes has generally been investigated by phase-contrast imaging and manual counting [27–29]. Flow cytometry, which has been used extensively in mammalian immune cell biology to help understand distinct immune cell types and functions, has been applied to *Galleria*, but flow plots vary widely across publications and methods use generally fixed, rather than live, immune cells [30–33]. Though fixation is vital for the detection of intercellular antigens via antibody staining, and for the attenuation of hazardous biological materials, fixatives have been shown to affect both relative cell size and granularity when analyzed by flow cytometry [34]. Thus, the use of fixative in the absence of meaningful antigen detection by antibody staining may not be entirely appropriate when investigating infection dynamics and phagocytosis.

Here, we present a method for the analysis of live *Galleria* haemocytes by flow cytometry with minimal sample processing. We demonstrate its efficacy in studying the phagocytosis of fluorescent particles and pathogens following injection into *Galleria* larvae and their subsequent incubation – meaning phagocytosis can be quantified over time. Finally, we show that this *in vivo* phagocytosis assay can detect the subversion of phagocytosis following  $\beta$ -glucan masking by *Candida albicans* grown on alternative carbon sources, which recapitulates *in vitro* cell culture data [35].

## Materials and methods

### *Galleria mellonella* rearing

An in-house colony of *Galleria mellonella* (under the banner of the *Galleria Mellonella* Research Centre, GMRC ([www.gmrcuk.org](http://www.gmrcuk.org))) was utilized for all experiments. All stages of the lifecycle were maintained in constant darkness at 30°C in a temperature-controlled incubator (LEEC). Briefly, 50 last instar larvae of indeterminate sex (as sexually dimorphic features in *Galleria* larvae have not yet been described) were placed into large PET jars with a small amount of larval diet (Jorjão et al. [36], diet recipe 3) and allowed to pupate. Following pupation, a folded piece of baking parchment was placed lengthways down into the jar to act as an attractive site for oviposition. Once eclosion and mating had occurred, fertilized embryos were collected from egg papers placed within the jars, and clutches of up to 300 were put into smaller PET jars containing 200–250 g of larval diet [36]. Larvae were allowed to develop undisturbed in these jars until needed for experiments.

### Larval injection

Last instar larvae were selected from larval feeding jars for use in experiments. Larvae between 250 and 350 mg were chosen, and those which showed either melanization or the presence of a bright dorsal ecdysial line [9] were omitted due to unsuitability for experiments. For injection, larvae were then held over a 1000  $\mu$ L pipette tip, ventral side up and 10  $\mu$ L of injectate mixture was injected using a Hamilton syringe (700 series – Merck) connected to a PB600 repeating syringe dispenser through the last right proleg for consistency. Following injection, larvae were kept within petri dishes according to the timepoint for analysis. Injected larvae were returned to temperature-controlled incubators as the time course began.

For control injections, *Galleria* larvae were injected with insect physiological saline (IPS – 150 mM sodium chloride, 5 mM potassium chloride, 10 mM tris HCl pH 6.9, 10 mM EDTA and 30 mM sodium citrate [37]). Uninjected controls were also used.

To identify *Galleria* phagocytes, pHrodo™ Red Zymosan Bioparticles™ were obtained as a 1 mg powder (ThermoFisher Scientific) and resuspended in 1 mL IPS to generate a final concentration of  $2 \times 10^7$  particles/mL. *Galleria* larvae were injected with 10  $\mu$ L, corresponding to a dose of  $2 \times 10^5$  particles.

### **E.Coli culturing**

Both the *E. coli* MG1655 control strain and mCherry strain were provided as kind gifts from Dr Remy Chait (University of Exeter). Strains were grown overnight at 37 °C with shaking (230 rpm) in LB broth. Suspensions were then centrifuged at 10,500  $\times$ g for 1 minute in pre-weighed Eppendorf tubes, resultant supernatants discarded, and the tubes re-weighed to calculate the mass of the bacterial cell pellets. The pellets were resuspended and plated on LB Agarose as serial dilutions and resultant colonies counted. This procedure was repeated three-fold in order to accurately relate cell pellet mass to CFU. On that basis, fresh overnight cultures were processed as above and resuspended in the appropriate volume of IPS to generate suspensions of final concentration  $3 \times 10^7$ ,  $1.5 \times 10^8$  or  $3 \times 10^8$  CFUs/mL. *Galleria* were injected with 10  $\mu$ L of the relevant bacterial suspension.

### **Candida albicans culturing**

*C. albicans* SC5314 [38] cultures were grown at 30 °C with shaking (200 rpm) in Yeast Nitrogen Base without amino acids (Merck) prepared according to the manufacturer's instructions, containing either 2% glucose, 2% glucose + 2% D/L-lactate (Merck), or 2% D/L-lactate alone [35].

### **pHrodo™ conjugation of E.Coli and C.Albicans**

Suspensions of *E. coli* and *C. albicans* were fixed for 20 minutes in 4% Paraformaldehyde diluted in PBS at room temperature with gentle agitation. The bacteria/fungi were then pelleted by centrifugation at 10,500  $\times$ g for 1 minute and the fixative removed. The pellet was washed and resuspended sequentially three times in PBS to remove residual fixative. pHrodo™ Red succinimidyl ester (ThermoFisher Scientific) was resuspended in DMSO and conjugated to the fixed pathogens

according to the manufacturer's instructions. Once the conjugation was completed, the samples were centrifuged at 10,500  $\times$ g for 1 minute, resuspended in IPS for injection into *Galleria* larvae. The *E. coli* pellet was resuspended to a final concentration of  $3 \times 10^7$ ,  $1.5 \times 10^8$  or  $3 \times 10^8$  CFUs/mL for inoculation. The *C. albicans* pellet was resuspended to a final concentration of  $3 \times 10^7$ ,  $7.5 \times 10^7$  or  $1.5 \times 10^8$  CFUs/mL for inoculation.

### **Hemolymph collection**

100  $\mu$ L of IPS supplemented with 1 mM phenolthiourea (PTU – Merck) in Eppendorfs was pre-chilled on ice prior to the start of haemolymph collection. *Galleria* larvae were removed from experimental petridishes and were held firmly and close to the lid of a clean petridish for haemolymph collection. The cuticle was pierced laterally on the larval thorax using a pointed scalpel blade, and the haemolymph was allowed to pool onto the petridish lid following gentle squeezing of the insect body. Once spent, the larval carcass was discarded and the haemolymph was immediately collected using a pipette and placed into the pre-chilled IPS +1 mM PTU solution. The haemolymph was mixed into the IPS solution by gentle pipetting, and the sample was placed back on ice when sufficiently dispersed. Between 3 and 5 larvae were bled and collected into a single sample tube depending on the experiment.

### **Hemolymph preparation for flow cytometry**

To prepare haemolymph samples for analysis by flow, the entire collected sample was passed through a 50  $\mu$ m CellTrics filter (WolfLabs Ltd) into a 5 mL round bottom tube. The filter was washed through with an extra 800  $\mu$ L of IPS +1 mM PTU solution, and the tube and filter were gently tapped on the work surface to encourage flow through where needed, and the sample was placed on ice. A 400  $\mu$ L aliquot of each sample was placed into a second 5 mL tube for staining with pHrodo™ Green at 1:2000 (CMG, ThermoFisher Scientific), for uniform staining of the plasma membrane (based on amphiphilic property of CMG) and/or 4',6-Diamidino-2'-phenylindole dihydrochloride at 1:1000 (DAPI, Merck) (as a cell impermeant fluorescent dye identifying dead cells based on binding double stranded DNA).

### **Flow cytometry analysis**

All analysis was carried out using an Attune NxT Flow Cytometer (Thermo Fisher Scientific). For each

starting sample, both stained and unstained aliquots were analysed. A total of 10,000 events within the haemocyte single-cell gate per sample were collected (see gating strategy in [Figure 1](#); Supplementary Figure S1), and the sample was analysed at a flow rate of 100  $\mu\text{L}/\text{min}$ . The haemocyte population on the FSC-H/SSC-H plot (scatter signals) was identified based on relative size/granularity as well as using CMG positive and DAPI negative features (see Supplementary Figure S1). These events were also corroborated by checking the haemocyte preparation in a microscope (data not shown). FCS files were exported to FlowJo (BD Biosciences) for subsequent interrogation and plot visualization. Data values were imported into GraphPad 9 (Prism) for statistical analysis and graphical representation.

### Confocal imaging of *ex vivo* haemocytes

Haemocytes from pHrodo zymosan injected *Galleria* were collected as described above for haemolymph collection, into 500  $\mu\text{L}$  of IPS +1 mM PTU solution. For observation by confocal microscopy, haemocytes were adhered to glass coverslips by centrifugation of the haemolymph samples using six well plates to house and spin the samples and coverslips. Plates were spun at 500  $\times g$  for 10 minutes at 4  $\mu\text{C}$  using a centrifuge with plate adapters. An additional IPS +1 mM PTU solution was gently added after spinning to the side of the well to wash away any unattached cells.

Prior to imaging, coverslips were removed from wells and placed cell side down onto a microscope slide and secured in place using nail polish. Samples were immediately imaged on a Zeiss LSM 880 AiryScanner confocal using a  $\times 40$  lens (NA 1.3). Z-stacks were acquired through the depth of the adhered cells at a step size of 0.5  $\mu\text{m}$ . Images were exported to FIJI for analysis and formatting.

### Statistical analyses

For statistical analysis, data were imported into GraphPad Prism 9. ANOVA and t-tests were completed dependent upon the experimental set-up. For all tests, ns indicates not significant ( $p > 0.05$ ), \* indicates  $p < 0.05$ , \*\* $p < 0.001$ , \*\*\* $p < 0.005$  and \*\*\*\* $p < 0.0001$ ) respectively. GraphPad Prism was also used to generate all graphs used in Figures throughout.

Experimental diagrams were created using BioRender.com. Diagrams, graphs and flow plots were imported into Adobe Photoshop for Figure building.

## Results

### Development of a *Galleria* live hemocyte flow cytometry pipeline

To investigate whether *Galleria* haemolymph centrifugation has any adverse effects on haemocyte cell profiles observed by flow cytometry, a haemolymph collection pipeline was developed ([Figure 1a](#)). Briefly, after haemolymph collection, the sample was filtered, before being split into two aliquots. The first – the “filtered” sample – was then immediately analysed, whilst the second was centrifuged at 500  $\times g$  for 5 minutes before being resuspended in IPS to form the “centrifuged” sample. By comparing aliquots from a single starting sample, differences in flow plot profiles could be attributed to post-collection processing, rather than sample variation.

Initial interpretation of the Forward and Side Scatter (FSC/SSC) plots from both filtered and centrifuged samples revealed a single area of density corresponding to the haemocytes within the sample. Thus, it appears that, in contrast to reports using fixed *Galleria* haemocytes [32,33], live *Galleria* haemocytes are not separable into sub populations based upon relative size and internal complexity alone.

Further analysis comparing post-collection processing methods revealed that the centrifugation and resuspension did not sufficiently remove debris (events outside of the haemocyte cell gate) from the sample or cause changes to the number of single-cell events detected ([Figure 1b,c](#)). However, the inclusion of DAPI to detect haemocyte cell death revealed that centrifugation causes a small, but significant, reduction in the number of single, living cells in the sample ([Figure 1d](#)). Together, [Figure 1b-d](#) illustrates the gating strategy employed for all subsequent experiments.

As distinct haemocyte subpopulations have previously been found by flow cytometry when fixed haemocyte samples are analysed [32,33], we repeated our protocol with the inclusion of 4% paraformaldehyde, following either the filtration or centrifugation steps (PFA, [Figure 1a](#)). Although there were no discernible differences in the haemocyte cell gate, a less dense secondary population did appear in both the centrifuged and fixed samples ([Figure 2a](#)). Using a stricter gating strategy, the secondary population could be gated separately from the main cell population, and the gate was superimposed across all samples to analyse the events within.

To determine the origin of the events within the secondary gate, we added a cell membrane dye (CellMask™ Green (CMG)) and DAPI (a non-permeable



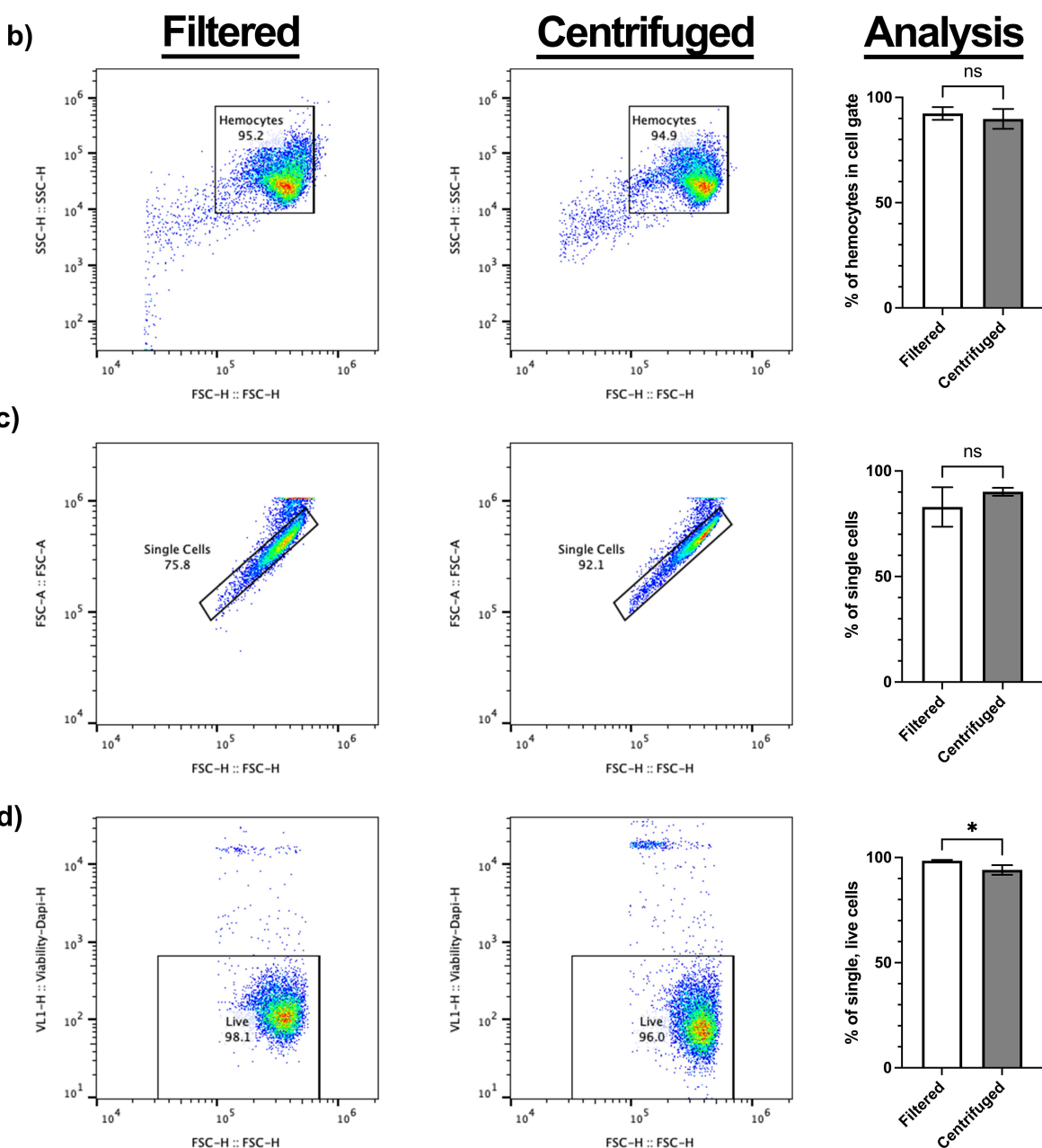
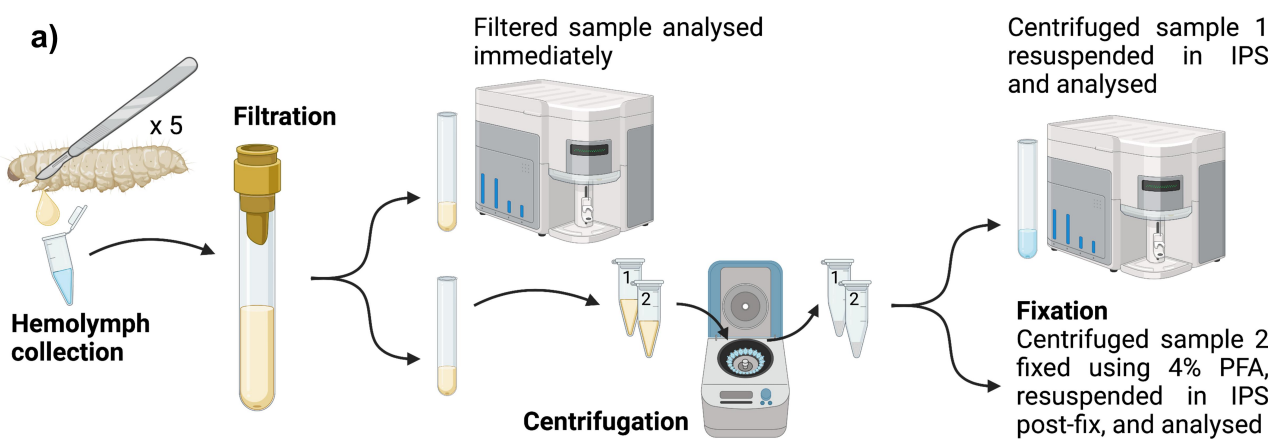


**Figure 1.** Collection method and analysis of galleria hemocytes by flow cytometry. a) schematic to show collection and processing methods of hemolymph collected from 5 galleria last instar larvae into a single sample. Samples were split two ways for analysis –

fluorescent DNA dye) to the samples prior to analysis. In the filtered only sample, non-cellular debris (CMG negative;DAPI negative) comprised the majority of events (Figure 2b – Q4, 69.6%) with the remaining events split between dead whole cells (CMG positive;DAPI positive) (Figure 2b - Q2) and free DNA-derived material; presumably from lysed cells (CMG negative;DAPI positive) (Figure 2B – Q1). As expected, a negligible fraction was CMG positive but DAPI negative – representing live cells that had evaded the primary gate (Figure 1 – Q3).

In relation to the filtered samples, a higher proportion of events in the secondary gate was observed for both the centrifuged and fixed samples (compare Figure 2a with 2A and A). Moreover, in the centrifuged only sample, the highest proportion of events were found within Q3 (Figure 2b). As the contents of Q3 are significantly increased following the process of centrifugation when compared to the filtered only sample, we suggest that centrifugation causes the contraction of living cells – which sees them fall out of the primary cell gate (Figure 2a-a) and into the secondary gate. Finally, the proportion of dead cells within the centrifuged sample also increased in relation to the filtered sample (Figure 2b-b, Q2), providing further evidence that centrifugation decreases the viability of haemocytes (Figure 1d).

No apparent changes in the haemocyte profile within the cell gate were observed following fixation of the haemocyte sample (Figure 2a), in contrast to previous work showing *Galleria* haemocytes cluster based on relative size and internal complexity [29,30]. In the fixed sample, the majority of the events in the secondary gate appear within the CMG+, Dapi-quartile (Figure 2b', Q3). As all fixed cells should readily take up Dapi, these events likely represent burst, anuclear cells. Only 20% of the events within the secondary gate had a cellular signature (Figure 2b – CMG+, Dapi+, Q2) – representing just 2% of the total events observed for the fixed sample.

These results suggest that post-collection processing methods such as centrifugation and fixing decrease the viability of *Galleria* haemocytes isolated from the circulating haemolymph. They also demonstrate that haemocytes form a single cluster based on relative size and internal complexity when analysed by flow cytometry.

## Using live haemocyte flow cytometry to quantify phagocytosis

As the scatter profiles of live *Galleria* haemocytes failed to distinguish sub-populations of innate immune cells, we sought to identify phagocytes based on the uptake of fluorescent particles. To achieve this, we injected a dose of  $2 \times 10^5$  pH sensitive zymosan particles (pHrodo™ Red) into last instar larvae, recovering the haemolymph after 2, 4 or 24 hrs (Figure 3a). Confocal imaging revealed fluorescent particles within haemocytes after 2 hrs, and 4 hrs, but with very few cells containing fluorescence after 24 hrs (Figure 3b). As the pH sensitive nature of the pHrodo™ dye means it only fluoresces when internalized, due to the lower pH inside the phagolysosomal system, we conclude that a proportion of the haemocytes constitute phagocytes, which are capable of degrading the zymosan particles over 24 hrs.

To further quantify their uptake, we next subjected live haemocyte samples injected with zymosan particles to flow cytometry, according to our filtration protocol (Figure 1a). Following gating for live, single haemocytes, the gated cells were further analysed for the presence of the pHrodo™ signal. The signal could indeed be detected within the haemocytes (Figure 3c), following a similar time-dependent profile to that observed by confocal microscopy. Analysis of the data revealed that the majority of particles were already taken up by 2 hours post injection (hpi), and that they had been predominantly cleared by 24 hpi (Figure 3d). Moreover, the mean fluorescence intensity (MFI) of the positive cell gate (Figure 3d) was significantly decreased at 24 hpi, in relation to 2 hrs, presumably corresponding to the processing and degradation of the particles over time.

As with total haemolymph (Figure 1b) the pHrodo™ positive phagocytes formed a single cluster based on relative size (FSC) and internal complexity (SSC) (Figure 3e). To determine whether the phagocytic haemocytes clustered within the entire haemocyte population, the pHrodo™ positive cells were overlaid onto the initial FSC-SSC scatter plot. This revealed that the phagocytes did not form an identifiable cluster and were relatively uniform throughout the main

---

filtrated hemolymph only and centrifuged hemolymph. Created using BioRender.com. b) comparative SSC vs FSC plots for filtered and centrifuged hemolymph. Centrifugation of hemolymph does not significantly concentrate hemocytes into the user-defined cell gate. c) gating strategy of single cells via visualisation of forward scatter height (FSC-H) to forward scatter area (FSC-A), comparing filtered and centrifuged samples. Centrifugation has no significant effect on the number of single cells in the sample. d) the number of live cells in each sample was determined by the inclusion of DAPI in the hemolymph sample. Centrifugation was found to significantly increase (\*,  $p < 0.05$ ,  $n = 3$  samples, each containing 5 larvae, unpaired t test) the number of dead cells within the sample.

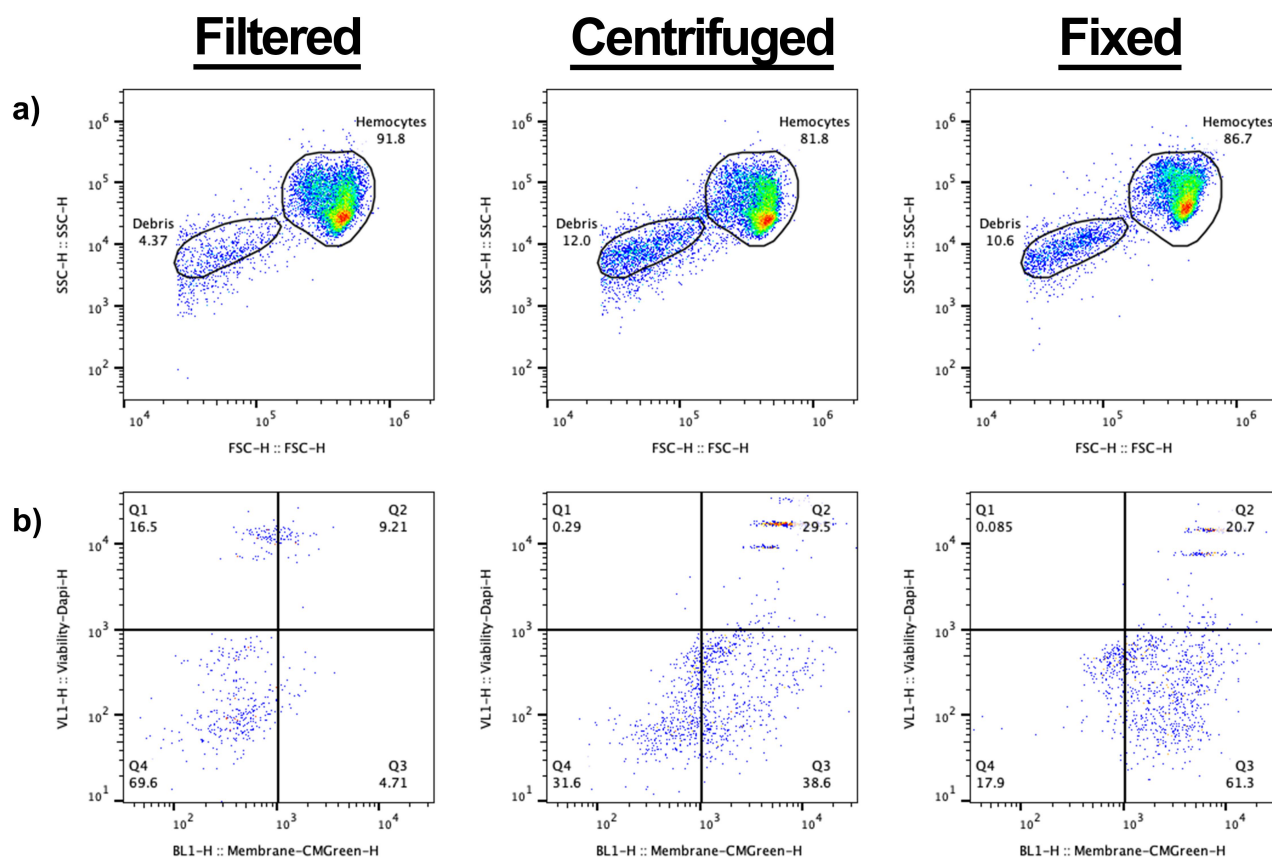


**Figure 2.** Analysis of non-cellular events within Galleria hemolymph. a) scatter to demonstrate the increase of non-cellular events following centrifugation and fixation of splits of the same starting sample. The non-cellular gate is designated 'debris'. b) analysis of events in the debris gate using a cell membrane dye – CMG, and DAPI. Q1 represents CMG negative, DAPI positive, Q2 represents CMG positive, DAPI positive – therefore dead cells –, Q3 represents CMG positive, DAPI negative – therefore live cells –, and Q4 represents CMG negative, DAPI negative – true, non-cellular 'debris'. In the filtered only sample, most events (69.6%) in the debris gate are deemed not cells (Q4). The profile dramatically changes following centrifugation – with more events becoming CMG positive (Q2 and Q3).

haemocyte cluster (Figure 3e – red events represent pHrodo™ cells, blue events represent the total sample). We therefore conclude that functional, live *Galleria* haemocyte populations cannot be characterized based on relative size and internal complexity alone.

### Using live haemocyte flow cytometry to monitor infection dynamics

We next sought to apply our live haemocyte flow pipeline to live bacteria, in order to investigate its efficacy in monitoring infection dynamics. *Escherichia coli* (*E. coli*) constitutively expressing chromosomally encoded mCherry were injected into last instar larvae, with haemolymph collected, filtered, and subjected to flow cytometry 1, 2, 4, 6 or 24 hr post injection. As with pHrodo™ zymosan, the fluorescent mCherry signal could be identified within single, live haemocytes (Figure 4a).

To investigate the maximum phagocytic capacity of haemocytes responding to a live bacterial infection, we

injected different doses of fluorescent *E. coli* into the larvae, prior to flow cytometry. All injection doses –  $3 \times 10^7$ ,  $1.5 \times 10^8$  or  $3 \times 10^8$  CFUs/mL – showed maximal uptake of fluorescent bacteria at 1 hpi, indicating rapid engulfment of the invading pathogen by the *Galleria* immune cells (Figure 4a,b). Interestingly, while the number of haemocytes containing mCherry *E. coli* increased in a dose-dependent manner at 1 hpi (Figure 4b), this trend was not apparent from 2 hpi onwards in the higher concentration ( $1.5 \times 10^8$  and  $3 \times 10^8$  CFUs/mL) samples, suggesting processing and degradation of the pathogen occurs within this timeframe. Moreover, although the maximum percentage of live, single haemocytes containing fluorescent *E. coli* increased with increasing dose at 1 hpi, this was not linear; 63.2% ( $\pm 1.2$   $N = 3$ ) of haemocytes injected with  $1.5 \times 10^8$  CFUs/mL contained fluorescent particles while 78.2% ( $\pm 1.5$   $N = 3$ ) of haemocytes injected with  $3 \times 10^8$  CFUs/mL contained fluorescent bacteria. It is therefore likely that the maximum phagocytic capacity of the *Galleria* immune cell repertoire plateaus at ~80%.

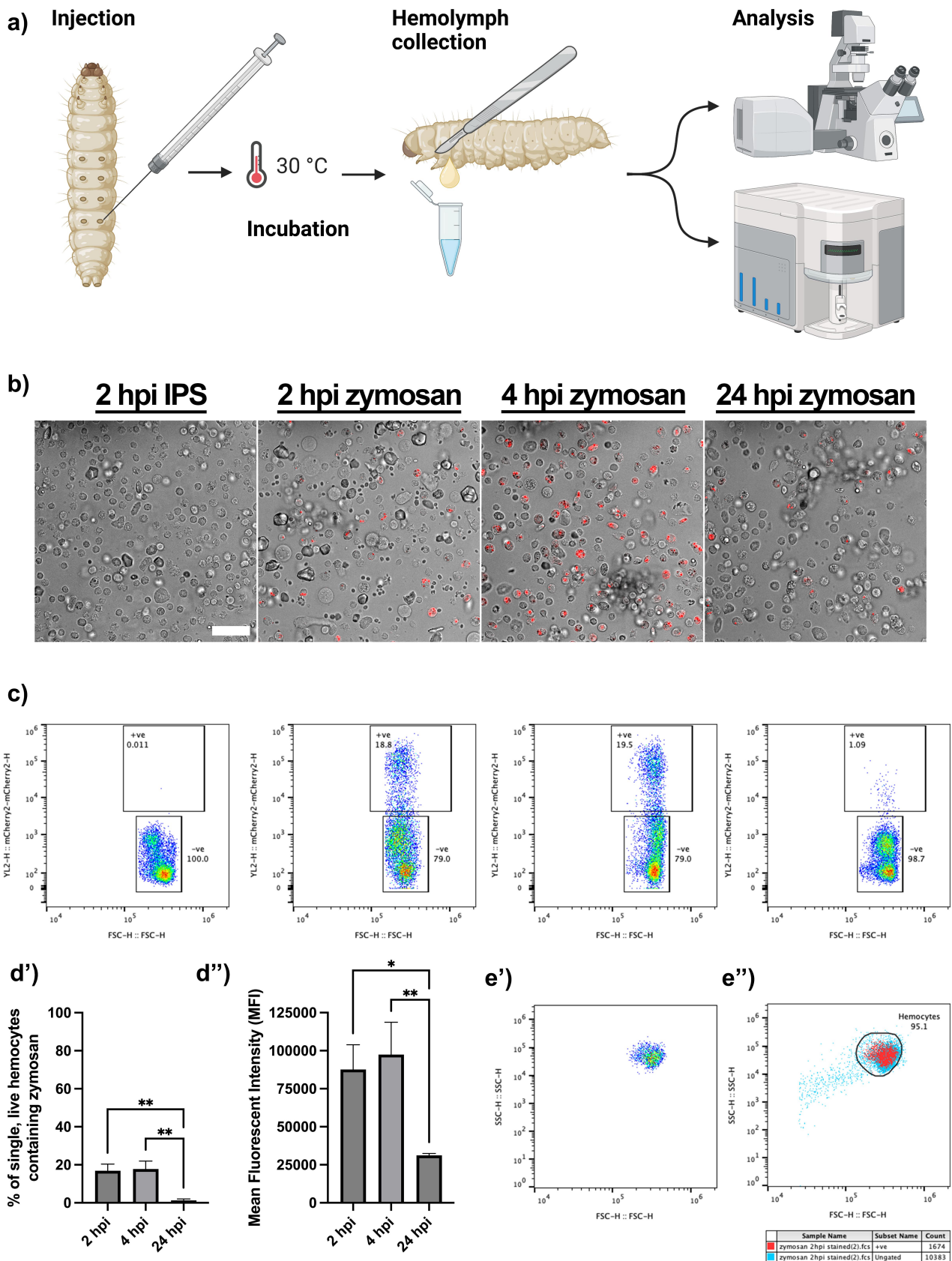


**Figure 3.** Identifying Galleria phagocytes by the uptake of fluorescent pHrodo™ zymosan particles. a) schematic to show injection pipeline through to analysis. Following injection with pHrodo™ zymosan particles, Galleria were returned to 30°C (rearing temperature) for incubation, before hemolymph was collected for analysis at set timepoints. Created using BioRender.com. b) hemocytes from injected larvae visualised by confocal microscopy. Phagocytosed zymosan particles (red) are seen at 2, 4 and



To investigate whether the *E. coli* strain used influenced haemocyte viability, we quantified the number of DAPI positive single cells in each sample. This revealed dose-dependent significant differences in the number of dead haemocytes at both the 1 and 24 hpi timepoints – with the highest percentage of dead cells ( $2.5\% \pm 0.346$ ,  $N = 3$ ) found at 24 hpi in samples from larvae injected with  $3 \times 10^8$  CFUs/mL *E. coli*. Intra-dose analysis further revealed a significant accumulation of dead cells over time in the  $3 \times 10^8$  CFUs/mL injection dose at 6 hpi ( $p < 0.001$ , 2-way ANOVA) and 24 hpi ( $p < 0.0001$ , 2-way ANOVA), and a significant reduction in the number of dead cells observed in the  $1.5 \times 10^8$  CFUs/mL injection dose when comparing 1 and 24 hpi ( $p < 0.05$ , 2-way ANOVA). At all other time points for all doses, the number of dead haemocytes in the samples remained statistically similar ( $p > 0.05$ ) indicating that haemocytes are rapidly able to deal with non-pathogenic *E. coli* through the phagolysosomal system without significant detriment to the number of live cells within the haemocyte repertoire.

### Using live haemocyte flow cytometry to quantify phagocytosis of fixed fluorescent pathogens

As *Galleria* larvae are used as a host for a wide range of pathogens in microbiological studies, we considered that not all researchers may have an appropriate fluorescent strain of their pathogen of interest. Therefore, we sought to determine whether fixed and labelled pathogens could also be analyzed for phagocytic uptake using our developed live cell haemocyte analysis pipeline.

To retain specificity for phagocytic uptake, we purchased the pH sensitive pHrodo dye in a conjugatable form, pHrodo™ Red succinimidyl ester (pHrodo™ Red SE). *E. coli* were fixed with 4% paraformaldehyde, conjugated with pHrodo™ Red, SE, injected into *Galleria* larvae at a concentration of  $3 \times 10^8$  CFUs/mL and haemolymph extracted at 2 hpi. As with both pHrodo zymosan and live mCherry *E. coli*, a shift in red fluorescence was observed in single, live haemocytes

corresponding to the uptake of the fixed conjugated bacteria (Figure 5a). 62.03% ( $\pm 2.601$ ,  $N = 3$ ) of single, live haemocytes contained fixed bacteria; similar to the proportion of single, live haemocytes containing live mCherry bacteria at the 2 hpi timepoint following an injection at  $3 \times 10^8$  CFUs/mL ( $65.97\% \pm 4.941$ ,  $N = 3$   $p < 0.2894$ , unpaired t test) (Figure 4b).

To assess whether this method could be utilized for other types of pathogens, pHrodo™ Red SE was conjugated to the pathogenic fungus *Candida albicans*. As with pHrodo-*E. coli*, uptake of *C. albicans* by *Galleria* haemocytes *in vivo* was indeed observed in a dose-dependent manner (Figure 5b and b). However, even at the highest dose ( $1.5 \times 10^8$  *Candida* cells/mL), only 48.10% ( $\pm 5.369$ ,  $N = 3$ ) of haemocytes had engulfed the labelled the fungal cells, whereas ~80% of haemocytes were able to engulf *E. coli* (Figure 4b). This is possibly due to the larger size of *C. albicans* yeast cells (volume approximately  $90 \mu\text{m}^3$  [35, 39] compared to *E. coli* (approximately  $1 \mu\text{m}^3$  [40]).

Finally, we sought to determine whether our method could identify and monitor biologically relevant differences in phagocytic uptake. The recognition of the major pathogen-associated molecular pattern,  $\beta$ -glucan, by pattern recognition receptors, such as dectin-1, is critical for phagocytic uptake and antifungal immunity in mammals [41]. However, *C. albicans* modulates immune recognition by masking  $\beta$ -glucan that has become exposed at the fungal cell surface in response to specific environmental signals, including lactate [35,42]. Thus, we exploited the process of  $\beta$ -glucan masking by *C. albicans* to test whether haemocytes, like mammalian macrophages, also display changes in phagocytic uptake in response to  $\beta$ -glucan masking [35,43,44]. Briefly, *C. albicans* SC5314 cells were grown in the presence or absence of glucose and lactate, before being fixed and conjugated to pHrodo™ Red SE. After conjugation, these differentially adapted *C. albicans* cells were injected into *Galleria* larvae at a concentration of  $3 \times 10^7$  *Candida* cells/mL. At 2 hpi, the haemolymph was extracted and the haemocytes analysed for phagocytic uptake of pHrodo-*C. albicans*. This revealed a significant decrease in phagocytosis of the  $\beta$ -glucan masked *C. albicans* cells grown in the presence of lactate, regardless of the inclusion of glucose

---

24 hours post injection (hpi). Scale bar at 50  $\mu\text{m}$ . c) scatter plots to show the proportion of live, single hemocytes containing pHrodo™ zymosan particles based on red fluorescence shift of events. d) quantification of phagocytosis over time via flow cytometry. There is a significant reduction in hemocytes containing particles at 24 hpi compared to be 2 and 4 hpi (\*\*,  $p < 0.01$ ,  $n = 3$  samples of 3 larvae per sample, one-way ANOVA with multiple comparisons). d') mean fluorescent intensity (MFI, arbitrary units) of events within the zymosan positive gate. MFI significantly decreases by 24 hpi (\*,  $p < 0.05$  and \*\*,  $p < 0.01$ ,  $n = 3$  samples of 3 larvae per sample, one-way ANOVA with multiple comparisons). E) Representative scatter plot of pHrodo™ positive hemocytes reveals a single cluster of cells based on relative size (FSC) and internal complexity (SSC). e') overlay of pHrodo™ positive hemocytes (red) onto the total hemocyte population (blue) reveals no distinct clustering of phagocytes within the entire hemocyte population.

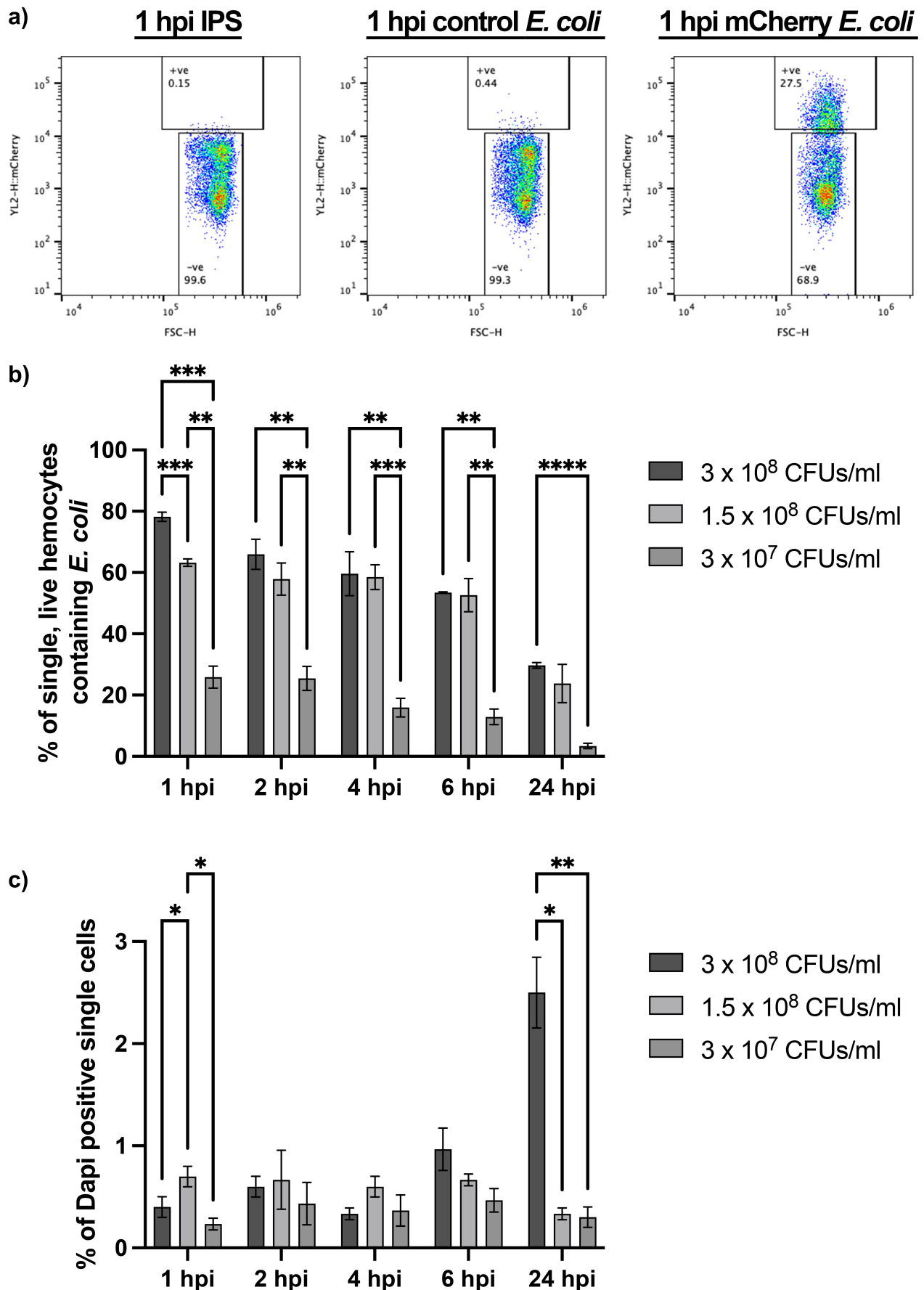


**Figure 4.** Understanding the response of *galleria* hemocytes to a live bacterial infection using mCherry *E. coli*. a) Representative scatter plots of single, live hemocytes from IPS control, control *E. coli* and mCherry *E. coli* injected *galleria* analysed at 1 hour post

(Figure 5c and c). This differential phagocytic uptake of masked and unmasked *C. albicans* cells faithfully replicates *in vitro* data using murine macrophages [44], thus demonstrating the reliability of the developed assay as well as the relevance of the *Galleria* infection model.

## Discussion

Over the last 20 years, larvae of the greater waxmoth, *Galleria mellonella*, have increased in popularity as the replacement and complementary model organism of choice for *in vivo* infections experiments in place of mammals. *Galleria* larvae have advantages over other non-mammalian models, such as *Drosophila* or zebra-fish larvae due to their relatively large size – which makes them easy to handle and dose – and the ability to raise them healthily at human physiological temperature.

The understanding of the immune cell repertoire of *Galleria* larvae dates back over 50 years [26], and little progress has been made to further characterize haemocyte subtypes, with reports focusing on cells that have been physically manipulated via either centrifugation or fixation. In this work, we sought to characterize live *Galleria* haemocytes by flow cytometry with the aim of quantifying distinct haemocyte subtypes following a minimal processing method in order to best maintain cell integrity and morphology.

In contrast with previous reports demonstrating separable sub-populations of fixed *Galleria* haemocytes based on relative size and internal complexity by flow cytometry [32], we found that live haemocytes subjected to a minimal processing method behaved as a single population, corroborating more recent methods to analyse fixed haemocytes by flow cytometry [31]. Even with the use of 4% PFA (Figure 2a) we failed to observe distinct haemocyte groups based on FSC and SSC. Instead, a single cluster of fixed cells was still observed with an accumulation of debris – with our FSC vs SSC plots showing remarkable similarity to other fixed *Galleria* haemocyte analysis [45], where researchers also gate a single population of cells separately from smaller and less complex events which appear on the flow plots. Whilst we cannot fully rule out that our described methodology, which includes a

filtration step, may be removing some populations of haemocytes, this seems unlikely. The filter diameter of 50  $\mu\text{m}$  used in the method exceeds that of the largest described haemocyte sub-population by 2.5-fold (oeno-cytoids at 19  $\mu\text{m}$ ) [46,47]. Similarly, whilst some haemocytes, such as plasmatocytes and granulocytes are known to be adherent [48] and may therefore stick to the filter, the loss of these cells would be identifiable following flow cytometry of centrifuged, unfiltered samples (Figure 2). Therefore, the simplest explanation for this discrepancy is that the previously described subpopulations of haemocytes [32] are artefacts from sample processing. This is supported by the observation that one of the assigned cell gates from previous work appears in the same vicinity as our described debris gate – which we have conclusively demonstrated does not contain viable haemocytes (Figure 2a,b). In addition, the use of fixatives has previously been reported to have an overall effect on cell morphology – as shown by clear differences in the FSC vs SSC scatter plots [31]. However, we do not rule out the possibility that the haemocyte landscape changes developmentally, as the larvae progress towards pupation, possibly resulting in a more complex distribution of cells the onset of metamorphosis [27].

As we show here, others have also observed a single haemocyte population by flow when live samples are analysed [30]. This work also reports a high level of cell death following centrifugation of the sample prior to analysis, which confirms our conclusion that filtration alone is preferable to maximize the number of viable cells for analysis within the haemolymph sample.

Having developed a minimal processing method for haemocyte analysis which maintains maximal cell integrity and viability, we sought to extend the assay to be able to quantify *in vivo* phagocytosis – an immune function of haemocytes that can be directly compared to mammalian immune responses. Fixed-cell flow cytometry has previously been used to measure *ex vivo* phagocytosis by *Galleria* haemocytes [33] where, again, designated haemocyte populations are not apparent in our live cell data. Meanwhile, other work conducting *ex vivo* [17,49,50] and *in vivo* [51] phagocytosis assays omit initial FSC/SSC plots and gating strategies – thus comparisons to the work presented here cannot be drawn – other than verifying that fluorescence shift can be

---

injection (hpi). Cells from larvae injected with mCherry *E. coli* show an increase in mCherry fluorescence detected (y axis). The shift in mCherry signal is specific to the chromosomally encoded mCherry *E. coli* strain. b) comparison of mCherry positive hemocytes across different injection doses. c) analysis of live cells across an infection timecourse and different injection doses. For all graphs statistical significance was determined using 2way ANOVA with Tukey's multiple comparisons. \*\*\*\* $p < 0.0001$ , \*\*\* $p < 0.001$ , \*\* $p < 0.01$  and \* $p < 0.05$ ,  $N=3$  samples of 3 larvae each for all doses and timepoints.

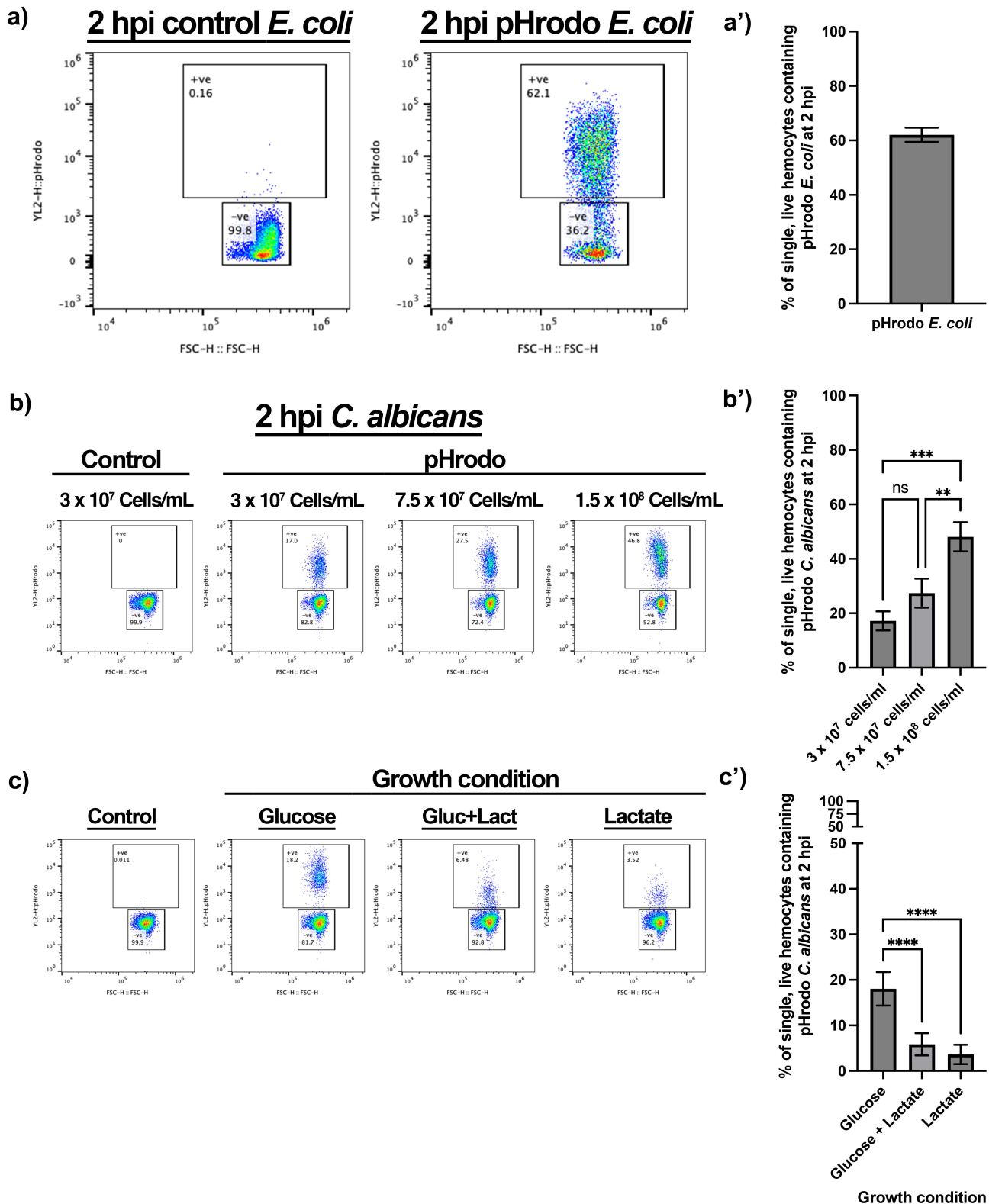


**Figure 5.** Monitoring fixed pathogen uptake following conjugation of pHrodo™ red SE. a) Representative flow plots show fluorescence shift following the uptake of pHrodo-*E. coli* by single, live hemocytes at 2 hours post injection (hpi). A') quantification of pHrodo-*E. coli* uptake,  $N=3$  samples of 3 larvae each. b) Representative flow plots of hemolymph analysed 2 hpi post fixed pHrodo-*C. albicans* at increasing doses compared to  $3 \times 10^7$  *Candida* cells/mL control fixed *C. albicans*. B') quantification of dose-dependent uptake of fixed pHrodo-*C. albicans*. Significance determined by one-way ANOVA with Tukey's multiple comparisons,  $***p < 0.001$  and  $**p < 0.01$ ,  $N=3$  samples containing 3 larvae for each dose. c) Representative flow plots of pHrodo-*C. albicans* uptake at 2 hpi by single, live hemocytes following growth in the presence of different sugar sources, in comparison to control. C') quantification of uptake comparing *C. albicans* growth conditions prior to fixation and conjugation. Significance determined by one-way ANOVA with Tukey's multiple comparisons.  $****p < 0.0001$ ,  $N=11$  samples for glucose and glucose + lactate, and  $N=10$  samples for lactate, each from 3 larvae per sample.



detected by flow cytometry in haemocytes that have performed phagocytosis of labelled pathogens.

Using our fluorescent phagocytosis assay, we have concluded that the maximum phagocytic capacity of the entire *Galleria* haemocyte repertoire is up to 80% (Figure 4B). This figure corresponds closely to previous work which calculates that the majority of *Galleria* haemocytes can be classed as either granular cells or plasmatocytes based on phenotypic observations [27] – both of which have further been shown to display phagocytic capability *in vitro* [23,29]. Unfortunately, combining these observations and our fluorescent particle uptake assay did not allow for the resolution of less abundant haemocyte subtypes – oenocytoids and spherulocytes – within the haemolymph by flow cytometry via backgating of the phagocytic cells (Figure 3E), which may indicate not only their low abundance, but also their heterogeneity. It is therefore likely that future work to characterize the less abundant haemocyte subtypes by flow cytometry may need to include the use of specific antibody staining, until such time that distinct haemocyte fluorescent reporter lines are generated by transgenesis – a method which allows for specific haemocyte subpopulation evaluation in *Drosophila melanogaster* [52].

Though phagocytic immune cell responses are undoubtedly better assayed in response to a live infection, it may often be the case that a fluorescent pathogen of interest is either not easily available or achievable, or that the fluorescence expression is linked to a gene promoter with transient or inducible expression. Through the fixation and pHrodo™ tagging of *C. albicans* for use in our *in vivo* *Galleria* phagocytosis assay we have demonstrated the suitability for this method in fixed pathogen uptake (Figure 5). Our analysis of insect haemocytes faithfully replicates previously published data showing that *C. albicans* uptake by mammalian phagocytes is strongly influenced by the masking of  $\beta$ -glucan at the fungal cell surface [44]. This is significant because  $\beta$ -glucan masking is thought to represent a means of immune evasion for this major fungal pathogen as it encounters certain host signals in specific niches [53–55].

In conclusion, here we present a rapid method to analyse the immune cell repertoire and assay phagocytosis in *in vivo* partial replacement model – *Galleria mellonella*. We demonstrate that this method is superior to previous attempts to analyse *Galleria* fixed or centrifuged *Galleria* immune cells due to improved cell viability and integrity. We corroborate previous findings which demonstrate that the majority of *Galleria* immune cells display phagocytic capability, and detail how the assay can be used to quantify phagocytosis over time – an immune response which, unlike the melanization of the organism, is relevant to mammalian immune responses. Moreover, the assay

developed here produces statistically significant results with only 30 larvae used per condition – representing a reduction of numbers of a model already used as a mammalian replacement, thus further refining the *Galleria* infection model in line with 3Rs principles [56].

## Acknowledgements

We would like to Ivan Canada Luna for his help in maintenance of the *Galleria* laboratory colony, and for stimulating discussions. We also thank Remy Chait (Biosciences, University of Exeter) for his provision of the *E. coli* strains used in this work. This work was funded by an NC3Rs Project Grant awarded to JGW and AJPB (NC/T001518/1), which supported JSC, and an NC3R Training Fellowship, awarded to JP (NC/W002388/1). AJPB was also funded by grants from the Medical Research Council UK (MR/M026663/2) and Wellcome (224323/Z/21/Z), and AP and AJPB were supported by the Medical Research Council Centre for Medical Mycology (MR/N006364/2).

## Disclosure statement

No potential conflict of interest was reported by the author(s).

## Funding

The work was supported by the Medical Research Council [MR/M026663/2]; Medical Research Council Centre for Medical Mycology [MR/N006364/2]; National Centre for the Replacement, Refinement and Reduction of Animals in Research [NC/T001518/1]; Wellcome Trust [224323/Z/21/Z]; NC3R [NC/W002388/1].

## Contributor roles

JSC – conceptualization, methodology, investigation, formal analysis, project administration and writing (review & editing); JCP – conceptualization and writing (editing); AB – methodology, formal analysis, writing (review & editing); AP: methodology, resources, writing (review & editing); RY – methodology, formal analysis, writing (review & editing); AJPB – conceptualization, methodology, resources, writing (review & editing), supervision, funding acquisition; JGW – conceptualization, methodology, project administration, writing (review & editing), supervision, funding acquisition.

## Data Availability statement

Raw data were generated at the Exeter Centre for Cytomics, UK. Derived data supporting the findings of this study are available from the corresponding author JGW/JSC on request.

## ORCID

James G. Wakefield  <http://orcid.org/0000-0003-3616-2346>

## References

- [1] Gladstone M, Li Y, Spiropoulos J, et al. *Galleria mellonella* - a novel infection model for the mycobacterium tuberculosis complex. *Virulence*. 2018;9(1):1126–1137. doi: [10.1080/21505594.2018.1491255](https://doi.org/10.1080/21505594.2018.1491255)
- [2] Norville IH, Hartley MG, Martinez E, et al. *Galleria mellonella* as an alternative model of *Coxiella burnetii* infection. *Microbiology*. 2014;160(6):1175–1181. doi: [10.1099/mic.0.077230-0](https://doi.org/10.1099/mic.0.077230-0)
- [3] Sheehan G, Kavanagh K. Proteomic analysis of the responses of *Candida albicans* during infection of *Galleria mellonella* larvae. *J Fungi Basel, Switzerland*. 2019.
- [4] Durieux M-F, Melloul É, Jemel S, et al. *Galleria mellonella* as a screening tool to study virulence factors of *Aspergillus fumigatus*. *Virulence*. 2021;12(1):818–834. doi: [10.1080/21505594.2021.1893945](https://doi.org/10.1080/21505594.2021.1893945)
- [5] Sheehan G, Clarke G, Kavanagh K. Characterisation of the cellular and proteomic response of *Galleria mellonella* larvae to the development of invasive aspergillosis. *BMC Microbiol*. 2018;18(1):63. doi: [10.1186/s12866-018-1208-6](https://doi.org/10.1186/s12866-018-1208-6)
- [6] Garcia-Bustos V, Pemán J, Ruiz-Gaitán A, et al. Host-pathogen interactions *Candida auris* infection: fungal behaviour and immune response in *Galleria mellonella*. *Emerg Microbes Infect*. 2022;11(1):136–146. doi: [10.1080/22221751.2021.2017756](https://doi.org/10.1080/22221751.2021.2017756)
- [7] Senior NJ, Bagnall MC, Champion OL, et al. *Galleria mellonella* as an infection model for *Campylobacter jejuni* virulence. *J Med Microbiol*. 2011;60(5):661–669. doi: [10.1099/jmm.0.026658-0](https://doi.org/10.1099/jmm.0.026658-0)
- [8] Wagley S, Borne R, Harrison J, et al. *Galleria mellonella* as an infection model to investigate virulence of *Vibrio parahaemolyticus*. *Virulence*. 2018;9(1):197–207. doi: [10.1080/21505594.2017.1384895](https://doi.org/10.1080/21505594.2017.1384895)
- [9] Wojda I, Staniec B, Sulek M, et al. The greater wax moth *Galleria mellonella*: biology and use in immune studies. *Pathog Dis*. 2020;78(9). doi: [10.1093/femspd/ftaa057](https://doi.org/10.1093/femspd/ftaa057)
- [10] Cerenius L, Söderhäll K. The prophenoloxidase-activating system in invertebrates. *Immunol Rev*. 2004;198(1):116–126. doi: [10.1111/j.0105-2896.2004.00116.x](https://doi.org/10.1111/j.0105-2896.2004.00116.x)
- [11] Tang H. Regulation and function of the melanization reaction in *Drosophila*. *Fly (Austin)*. 2009;3(1):105–111. doi: [10.4161/fly.3.1.7747](https://doi.org/10.4161/fly.3.1.7747)
- [12] Loh JMS, Adenwalla N, Wiles S, et al. *Galleria mellonella* larvae as an infection model for group A streptococcus. *Virulence*. 2013;4(5):419–428. doi: [10.4161/viru.24930](https://doi.org/10.4161/viru.24930)
- [13] Brown SE, Howard A, Kasprzak AB, et al. A peptidomics study reveals the impressive antimicrobial peptide arsenal of the wax moth *Galleria mellonella*. *Insect Biochem Mol Biol*. 2009;39(11):792–800. doi: [10.1016/j.ibmb.2009.09.004](https://doi.org/10.1016/j.ibmb.2009.09.004)
- [14] Mak P, Zdybicka-Barabas A, Cytryńska M. A different repertoire of *Galleria mellonella* antimicrobial peptides in larvae challenged with bacteria and fungi. *Dev Comp Immunol*. 2010;34(10):1129–1136. doi: [10.1016/j.dci.2010.06.005](https://doi.org/10.1016/j.dci.2010.06.005)
- [15] Lavine MD, Strand MR. Insect hemocytes and their role in immunity. *Insect Biochem Mol Biol*. 2002;32(10):1295–1309. doi: [10.1016/S0965-1748\(02\)00092-9](https://doi.org/10.1016/S0965-1748(02)00092-9)
- [16] Musselman LP, Fink JL, Ramachandran PV, et al. Role of fat body lipogenesis in protection against the effects of caloric overload in *Drosophila*. *J Biol Chem*. 2013;288(12):8028–8042. doi: [10.1074/jbc.M112.371047](https://doi.org/10.1074/jbc.M112.371047)
- [17] Wu G, Liu J, Li M, et al. Prior infection of *Galleria mellonella* with sublethal dose of bt elicits immune priming responses but incurs metabolic changes. *J Insect Physiol*. 2022;139:104401. doi: [10.1016/j.jinsphys.2022.104401](https://doi.org/10.1016/j.jinsphys.2022.104401)
- [18] Mowlds P, Kavanagh K. Effect of pre-incubation temperature on susceptibility of *Galleria mellonella* larvae to infection by *Candida albicans*. *Mycopathologia*. 2008;165(1):5–12. doi: [10.1007/s11046-007-9069-9](https://doi.org/10.1007/s11046-007-9069-9)
- [19] Asai M, Sheehan G, Li Y, et al. Innate immune responses of *Galleria mellonella* to mycobacterium bovis BCG challenge identified using proteomic and molecular approaches. *Front Cell Infect Microbiol*. 2021;11:619981. doi: [10.3389/fcimb.2021.619981](https://doi.org/10.3389/fcimb.2021.619981)
- [20] Perdoni F, Falleni M, Tosi D, et al. A histological procedure to study fungal infection in the wax moth *Galleria mellonella*. *Eur J Histochem*. 2014;58(3):2428. doi: [10.4081/ejh.2014.2428](https://doi.org/10.4081/ejh.2014.2428)
- [21] Eleftherianos I, Heryanto C, Bassal T, et al. Haemocyte-mediated immunity in insects: cells, processes and associated components in the fight against pathogens and parasites. *Immunology*. 2021;164(3):401–432. doi: [10.1111/imm.13390](https://doi.org/10.1111/imm.13390)
- [22] Hultmark D, Andó I. Hematopoietic plasticity mapped in *Drosophila* and other insects. *Elife*. 2022;11:e78906. doi: [10.7554/eLife.78906](https://doi.org/10.7554/eLife.78906)
- [23] Tojo S, Naganuma F, Arakawa K, et al. Involvement of both granular cells and plasmatocytes in phagocytic reactions in the greater wax moth, *Galleria mellonella*. *J Insect Physiol*. 2000;46(7):1129–1135. doi: [10.1016/S0022-1910\(99\)00223-1](https://doi.org/10.1016/S0022-1910(99)00223-1)
- [24] Jiang H, Vilcinskas A, Kanost MR. Immunity in lepidopteran insects. *Adv Exp Med Biol*. 2010;708:181–204.
- [25] Zdybicka-Barabas A, Sowa-Jasiłek A, Stączek S, et al. Different forms of apolipoprotein III in *Galleria mellonella* larvae challenged with bacteria and fungi. *Peptides*. 2015;68:105–112. doi: [10.1016/j.peptides.2014.12.013](https://doi.org/10.1016/j.peptides.2014.12.013)
- [26] Ratcliffe NA, Gagen SJ. Studies on the in vivo cellular reactions of insects: an ultrastructural analysis of nodule formation in *Galleria mellonella*. *Tissue Cell*. 1977;9(1):73–85. doi: [10.1016/0040-8166\(77\)90050-7](https://doi.org/10.1016/0040-8166(77)90050-7)
- [27] Wu G, Liu Y, Ding Y, et al. Ultrastructural and functional characterization of circulating hemocytes from *Galleria mellonella* larva: cell types and their role in the innate immunity. *Tissue Cell*. 2016;48(4):297–304. doi: [10.1016/j.tice.2016.06.007](https://doi.org/10.1016/j.tice.2016.06.007)
- [28] Gago S, García-Rodas R, Cuesta I, et al. *Candida parapsilosis*, *Candida orthopsilosis*, and *Candida metapsilosis* virulence in the non-conventional host *Galleria mellonella*. *Virulence*. 2014;5(2):278–285. doi: [10.4161/viru.26973](https://doi.org/10.4161/viru.26973)
- [29] Tomiotto-Pellissier F, Cataneo AHD, Orsini TM, et al. *Galleria mellonella* hemocytes: A novel phagocytic assay for *Leishmania (Viannia) braziliensis*. *J Microbiol Methods*. 2016;131:45–50. doi: [10.1016/j.mimet.2016.10.001](https://doi.org/10.1016/j.mimet.2016.10.001)

- [30] Wrońska AK, Kaczmarek A, Kazek M, et al. Infection of *Galleria mellonella* (lepidoptera) larvae with the entomopathogenic fungus *conidiobolus coronatus* (entomophthorales) induces apoptosis of hemocytes and affects the concentration of eicosanoids in the Hemolymph. *Front Physiol.* 2022;12. doi: [10.3389/fphys.2021.774086](https://doi.org/10.3389/fphys.2021.774086)
- [31] Wrońska AK, Kaczmarek A, Sobich J, et al. Intracellular cytokine detection based on flow cytometry in hemocytes from *Galleria mellonella* larvae: a new protocol. *PLoS One.* 2022;17(9):e0274120. doi: [10.1371/journal.pone.0274120](https://doi.org/10.1371/journal.pone.0274120)
- [32] Browne N, Surlis C, Maher A, et al. Prolonged preincubation increases the susceptibility of *Galleria mellonella* larvae to bacterial and fungal infection. *Virulence.* 2015;6(5):458–465. doi: [10.1080/21505594.2015.1021540](https://doi.org/10.1080/21505594.2015.1021540)
- [33] García-García E, García-García PL, Rosales C. An fMLP receptor is involved in activation of phagocytosis by hemocytes from specific insect species. *Dev Comp Immunol.* 2009;33(6):728–739. doi: [10.1016/j.dci.2008.12.006](https://doi.org/10.1016/j.dci.2008.12.006)
- [34] Rousselle C, Robert-Nicoud M, Ronot X. Flow cytometric analysis of DNA content of living and fixed cells: a comparative study using various fixatives. *Histochem J.* 1998;30(11):773–781. doi: [10.1023/A:1002942418520](https://doi.org/10.1023/A:1002942418520)
- [35] Ballou ER, Avelar GM, Childers DS, et al. Lactate signalling regulates fungal  $\beta$ -glucan masking and immune evasion. *Nat Microbiol.* 2016;2(2):16238. doi: [10.1038/nmicrobiol.2016.238](https://doi.org/10.1038/nmicrobiol.2016.238)
- [36] Jorjão AL, Oliveira LD, Scorzoni L, et al. From moths to caterpillars: Ideal conditions for *Galleria mellonella* rearing for in vivo microbiological studies. *Virulence.* 2018;9(1):383–389. doi: [10.1080/21505594.2017.1397871](https://doi.org/10.1080/21505594.2017.1397871)
- [37] Fuchs BB, O'Brien E, Khoury JBE, et al. Methods for using *Galleria mellonella* as a model host to study fungal pathogenesis. *Virulence.* 2010;1(6):475–482. doi: [10.4161/viru.1.6.12985](https://doi.org/10.4161/viru.1.6.12985)
- [38] Gillum AM, Tsay EY, Kirsch DR. Isolation of the *Candida albicans* gene for orotidine-5'-phosphate decarboxylase by complementation of *S. cerevisiae* *ura3* and *E. coli* *pyrF* mutations. *Mol Gen Genet.* 1984;198(1):179–182. doi: [10.1007/BF00328721](https://doi.org/10.1007/BF00328721)
- [39] FM K, CG DK, Stanley B. Cell wall-related bionumbers and bioestimates of *Saccharomyces cerevisiae* and *Candida albicans*. *Eukaryot Cell.* 2014;13(1):2–9. doi: [10.1128/EC.00250-13](https://doi.org/10.1128/EC.00250-13)
- [40] Sajed T, Marcu A, Ramirez M, et al. ECMDDB 2.0: A richer resource for understanding the biochemistry of *E. coli*. *Nucleic Acids Res.* 2016;44(D1): D495–501. doi: [10.1093/nar/gkv1060](https://doi.org/10.1093/nar/gkv1060)
- [41] Brown GD, Gordon S. A new receptor for  $\beta$ -glucans. *Nature.* 2001;413(6851):36–37. doi: [10.1038/35092620](https://doi.org/10.1038/35092620)
- [42] Pradhan A, Avelar GM, Bain JM, et al. Non-canonical signalling mediates changes in fungal cell wall PAMPs that drive immune evasion. *Nat Commun.* 2019;10(1):5315. doi: [10.1038/s41467-019-13298-9](https://doi.org/10.1038/s41467-019-13298-9)
- [43] Ene IV, Adya AK, Wehmeier S, et al. Host carbon sources modulate cell wall architecture, drug resistance and virulence in a fungal pathogen. *Cell Microbiol.* 2012;14(9):1319–1335. doi: [10.1111/j.1462-5822.2012.01813.x](https://doi.org/10.1111/j.1462-5822.2012.01813.x)
- [44] Ene IV, Cheng S-C, Netea MG, et al. Growth of *Candida albicans* cells on the physiologically relevant carbon source lactate affects their recognition and phagocytosis by immune cells. *Infect Immun.* 2013;81(1):238–248. doi: [10.1128/IAI.01092-12](https://doi.org/10.1128/IAI.01092-12)
- [45] Wrońska AK, Boguś MI, Song L. Heat shock proteins (HSP 90, 70, 60, and 27) in *Galleria mellonella* (lepidoptera) hemolymph are affected by infection with *conidiobolus coronatus* (entomophthorales). *PLoS One.* 2020;15(2):e0228556. doi: [10.1371/journal.pone.0228556](https://doi.org/10.1371/journal.pone.0228556)
- [46] Elmekawy A, Elshehaby M, Saber S, et al. Evaluation of *Galleria mellonella* immune response as a key step toward plastic degradation. *J Basic Appl Zool.* 2023;84(1):27. doi: [10.1186/s41936-023-00349-3](https://doi.org/10.1186/s41936-023-00349-3)
- [47] Torres M, Pinzón EN, Rey FM, et al. *Galleria mellonella* as a Novelty in vivo Model of Host-Pathogen Interaction for *Malassezia furfur* CBS 1878 and *Malassezia pachydermatis* CBS 1879. *Front Cell Infect Microbiol.* 2020;10. doi: [10.3389/fcimb.2020.00199](https://doi.org/10.3389/fcimb.2020.00199)
- [48] Admella J, Torrents E. A straightforward method for the isolation and cultivation of *Galleria mellonella* hemocytes. *Int J Mol Sci.* 2022;23(21):13483. doi: [10.3390/ijms232113483](https://doi.org/10.3390/ijms232113483)
- [49] Zhang Y, Li J, Yu F, et al. Allograft inflammatory factor-1 stimulates hemocyte immune activation by enhancing phagocytosis and expression of inflammatory cytokines in *Crassostrea gigas*. *Fish Shellfish Immunol.* 2013;34(5):1071–1077. doi: [10.1016/j.fsi.2013.01.014](https://doi.org/10.1016/j.fsi.2013.01.014)
- [50] Sheehan G, Kavanagh K. Analysis of the early cellular and humoral responses of *Galleria mellonella* larvae to infection by *Candida albicans*. *Virulence.* 2018;9(1):163–172. doi: [10.1080/21505594.2017.1370174](https://doi.org/10.1080/21505594.2017.1370174)
- [51] Kim CH, Shin YP, Noh MY, et al. An insect multiligand recognition protein functions as an opsonin for the phagocytosis of microorganisms. *J Biol Chem.* 2010;285(33):25243–25250. doi: [10.1074/jbc.M110.134940](https://doi.org/10.1074/jbc.M110.134940)
- [52] Anderl I, Vesala L, Ihalainen TO, et al. Transdifferentiation and proliferation in two distinct hemocyte lineages in *Drosophila melanogaster* larvae after wasp infection. *PLOS Pathog.* 2016;12(7):e1005746. doi: [10.1371/journal.ppat.1005746](https://doi.org/10.1371/journal.ppat.1005746)
- [53] Pradhan A, Avelar GM, Bain JM, et al. Hypoxia promotes immune evasion by triggering  $\beta$ -glucan masking on the *Candida albicans* cell surface via mitochondrial and cAMP-protein kinase a signaling. *MBio.* 2018;9(6):e01318–18. doi: [10.1128/mBio.01318-18](https://doi.org/10.1128/mBio.01318-18)
- [54] Lopes JP, Stylianou M, Backman E, et al. Evasion of Immune Surveillance in Low Oxygen Environments Enhances *Candida albicans* Virulence. *MBio.* 2018;9(6). doi: [10.1128/mBio.02120-18](https://doi.org/10.1128/mBio.02120-18)
- [55] Childers DS, Avelar GM, Bain JM, et al. Epitope Shaving Promotes Fungal Immune Evasion. *MBio.* 2020;11(4):11. doi: [10.1128/mBio.00984-20](https://doi.org/10.1128/mBio.00984-20)
- [56] Russell WMS, Burch RL. The principles of humane experimental technique. Wheathampstead (UK): Universities Federation for Animal Welfare; 1959.